*Korean J. Chem. Eng.*, 34(11), 2978-2983 (2017)
DOI: 10.1007/s11814-017-0202-2

pISSN: 0256-1115
eISSN: 1975-7220

# Nitrogen doped graphene/cobalt-based catalyst layers of a PEM fuel cell: Performance evaluation and multi-objective optimization

**Bagher Kazeminasab*, Soosan Rowshanzamir**,***,†, and Hossein Ghadamian****

*Department of Energy Engineering, Graduate College of Environment and Energy, Science and Research Branch, Islamic Azad University, Tehran, Iran
**School of Chemical Engineering, Iran University of Science and Technology, Tehran, Iran
***Fuel Cell Laboratory, Green Research Center, Iran University of Science and Technology
****Department of Energy, Materials and Energy Research Center (MERC), Tehran, Iran
(*Received 22 February 2017 • accepted 24 July 2017*)

**Abstract**−The proton exchange membrane fuel cell could be made more commercially viable by substituting the expensive platinic catalyst without loss of performance. This should be done simultaneously through optimization and use of a non-precious metal catalyst. In this study, multi-objective optimization of the catalyst layer was done on non-precious metal catalysts. Nitrogen-doped graphene (NG)-based cobalt was synthesized as a non-precious metal catalyst. Differential equations were solved at the modeling stage by the shooting method, and objective functions were solved at the optimization stage using sequential quadratic programming. NG-based cobalt was evaluated in a cell and then compared with the platinum catalyst. Results present the synthesized non-precious catalyst as an appropriate replacement for existing precious metal catalyst. Also, the polarization curve demonstrates that the current modeling is in good agreement with NG-based cobalt catalyst. Finally, the Pareto curve at the voltage of 0.6 V (and 300 A/m$^2$ current density in the base case) indicated that the best tradeoff between cost and performance of the catalyst layer was achieved when the current density was increased in the range of 5% to 15%.

Keywords: PEM Fuel Cell, Multi-objective Optimization, Non-precious Catalyst, Nitrogen Doped Grapheme-based Cobalt, Pareto Curve

## INTRODUCTION

A catalyst layer (CL) is usually the slimmest layer in a PEM fuel cell; however this is an extremely complex component because of its porosity, several phases, and reactions [1]. An efficient catalyst layer should provide several functions at the same time: transporting the electrons and protons, supplying oxygen and hydrogen and water management. The structure and composition of the catalyst layer affect all these roles. Optimization of the catalyst layer can provide for all these requirements, as well as increase utilization of the catalyst, its durability and performance [2]. The high cost and scarcity of precious metals such as platinum is an obstacle to commercial application in anodes and cathodes. Research on ways to reduce cost and increase performance of a fuel cell has taken two routes: replacement of platinum with a proper non-precious catalyst [3] and optimal design of the fuel cell to predict and comprehend the phenomena that take place inside the cell.

Among the various different non-precious catalysts that have been studied to date, composites of carbons and transition metals have shown reasonable activity [3]. Introducing nitrogen atoms into different structures of carbonic net led to progress in electrochemical properties of this group of materials. In our previous work [4], among the evaluated non-precious catalysts, NG-based cobalt nanoparticle was selected as the best catalyst.

In total, an operational and affordable non-precious catalyst with adequate activity is desired. Synthesizing cobalt, then, onto the nitrogen-doped graphene via modified polyol method, could lead us to reach these goals.

After an appropriate non-precious catalyst was chosen, catalyst layer optimization was concerned. Primary works about optimization have investigated selection of a suitable model. Broka and Ekdunge were among the first to model the catalyst layer [5]. Their results showed that the agglomerate type model had the best agreement with empirical results compared to the pseudohomogeneous model, especially at high current density. Sui et al. modeled and optimized the catalyst layer and confirmed the above mentioned results [6]. Following surveys have evaluated parameters of the catalyst layer. For instance, Wang et al. studied the effect of structural parameters in the catalyst layer and determined oxygen diffusion coefficient, proton conductivity, and agglomerate size as key parameters [7]. Sun et al. accounted for catalyst layer thickness, catalyst loading, and ionomer content as the most important parameters [8]. Other studies focused on optimization of objective functions. Srinivasarao et al. researched optimization of the catalyst layer in terms of current density and cost of the catalyst layer separately as two objective functions. They reduced the cost power ratio by about 40% and improved performance by about 10% [9]. Kulikovsky et al. presented an optimized model for the catalyst layer and showed that

†To whom correspondence should be addressed.
E-mail: rowshanzamir@iust.ac.ir

optimal catalyst distribution had a more important effect than optimal ionomer distribution at high current density [10]. Recent studies have been directed toward multi objective optimization (MOO) of fuel cell systems. For example Mert, Feali and Ang et al. conducted MOO for direct methanol fuel cells [11], microfluid fuel cells [12], and PEM fuel cell systems [13], respectively. Hereafter, studies about MOO of fuel cells at the scale of system stopped and research have shifted toward a synthesizing a non-precious catalyst and improving determination of methods of effective CL parameters. Park et al. did empirical tests to optimize the CL composition of NG-based non-precious metal catalysts. They showed that electrodes with 66.7% and 50% of Nafion had the best performance as an oxidant in oxygen and air, respectively [14]. Malko et al. applied EIS test to determine the main parameters on CL performance, and then they prepared a simple flowchart for CL optimization with the least number by trial and error [15].

MOOs have been progressing in many sciences including energy and fuel cells, but so far they have not been conducted for the most complex and important part in a fuel cell, the catalyst layer. Also, all the performed MOOs were carried out on platinic catalyst even about fuel cell systems. Hence, it is necessary to apply this kind of optimization based on non-precious catalysts.

Generally, this study included MOO of the catalyst layer of a PEM fuel cell on the basis of a non-precious catalyst. In this work, a steady-state, isothermal, one-dimensional model with agglomerate structure was considered. After modeling, MOO of the catalyst layer was accomplished according to NG-based cobalt data.

## CATALYST LAYER MODELING

First, a steady-state, isothermal, one-dimensional model with agglomerate structure was developed to model the catalyst layer (Fig. 1). The produced non-linear differential equations in this stage were solved by the boundary value problem and the shooting method. Then at the optimization stage, MOO was solved using sequential quadratic programming and the min-max method; details for the platinic catalyst are presented in our previous work [16]. Objective functions were optimized under important or accountable variables through coding in MATLAB software and an fminimax common. Objective functions include current density and the cost of CL, and the variables include cobalt loading, ionomer volume fraction, agglomerate porosity and radius and water saturation. Written code can optimize many objective functions simultaneously, but here because of empirical limitations only two objective functions contain the current density and the cost were optimized.

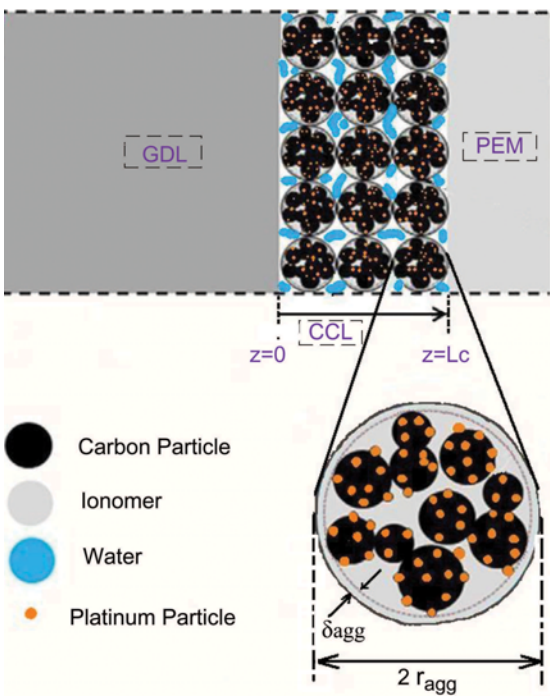


**Fig. 1. An agglomerated cathode catalyst layer of a PEM fuel cell [16].**

The objective functions are as equations below ($f_1$: current density function, $f_2$: CL cost function):

$$f_1 = -I_\delta \ [A/m^2] \tag{1}$$

$$f_2 = (C_1(W_{Co}+W_{NG})+C_2W_i) \ [\$] \tag{2}$$

$C_1$ is cost of cobalt (cobalt (II) nitrate hexahydrate; Merck) and nitrogen doped graphene (made from pentachloropyridine (Merck) and metallic potassium (Sigma-Aldrich) in our laboratory)=−15.3 $r_{Co/NG}$+19.35 \$/g

$C_2$ is cost of ionomer (Nafian 5% solution; Electrochem)=41.92 \$/g

Among fourteen structural and compositional parameters of the catalyst layer considered at the modeling stage, five important and key parameters (as mentioned above) are used as decision variables at the optimization stage. The lower and upper limits (LB and UB) of these variables are defined as below:

$$\begin{cases} X=[m_{Co}, L_{mc}, \varepsilon_{agg}, r_{agg}, s] \\ LB=[0.01, 0.01, 0.1, 0.01, 0.01] \\ UB=[5.0, 0.9, 0.9, 0.5, 0.9]; \end{cases} \tag{3}$$

Constraints could be put on objective functions or variables. First, constraints of variables are considered as volume fraction of solid, ionomer and void in the catalyst layer [9]:

$$\begin{cases} \varepsilon_v=\varepsilon_{CL}=1-\dfrac{m_{Co}}{t_{CL}r_{Co/NG}}\left(\dfrac{1-r_{Co/NG}}{\rho_c}+\dfrac{r_{Co/NG}}{\rho_{Co}}+\dfrac{L_{mc}}{(1-L_{mc})\rho_{Co}}\right) & 0<\varepsilon_v<1 \\ \varepsilon_i=L_{mc}=\dfrac{1}{t_{CL}\rho_i r_{Co/NG}}\dfrac{m_{Co}}{}\left(\dfrac{L_{mc}}{1-L_{mc}}\right) & 0<\varepsilon_i<1 \\ \varepsilon_s=1-\varepsilon_v-\varepsilon_i & 0<\varepsilon_s<1 \end{cases} \tag{4}$$

Second, constraints of objective functions could be defined as relations below:

$$\begin{cases} \text{Catalyst Layer Cost}_{Optimized} < \text{Catalyst Layer Cost}_{Base\ case} \\ \text{Current Density}_{Optimized} > 1.2 * \text{Current Density}_{Base\ case} \end{cases} \tag{5}$$

Finally, objective functions are calculated using fminimax command according to Eq. (6). This command is formed by objective

functions, variables and constraints as below:

$$\begin{cases} \text{fminimax } f_1, f_2 \\ \text{w.r.t.: } m_{Co}, L_{mc}, \varepsilon_{agg}, r_{agg}, s \\ \text{Subject to: } 0 \le \varepsilon_v \le 1,\ 0 \le \varepsilon_s \le 1,\ 0 \le \varepsilon_i \le 1 \end{cases} \quad (6)$$

## RESULTS AND DISCUSSION

### 1. Preparing the Experimental Data

It is necessary to provide non-precious catalyst data before validation takes place. Operational parameters such as temperature and pressure were set locally under experiment conditions. Parameters such as catalyst loading, catalyst mass fraction and Nafion fraction were determined during catalyst synthesis. Some structural parameters such as thickness of gas diffusion layer (GDL) and membrane were obtained from the vendor's catalogue or website and rechecked in the laboratory. Density of elements and volume fraction of GDL penetrating into the catalyst layer were derived from the mentioned articles. The thickness of the catalyst layer was specified from an SEM image of the cross section of the catalyst layer, and the size of the particles of the catalyst was determined using a TEM image. In sum, the required data are gathered in Table 1. Furthermore, to test the reliability of model at varying temperature and humidity, the fuel cell station was run in the following sections.

### 2. Experimental Setup

First, catalyst ink was made through loading 40 wt% Co on nitrogen doped graphene [4] solved in 5% nafion solution (Electrochem Inc). Then, the prepared catalyst ink was sprayed onto the carbon paper GDLs (Electrochem Inc.) with an active area of 5 $cm^2$ to make anode and cathode electrodes with 1 mgCo/$cm^2$ catalyst loading. Membrane electrode assemblies were fabricated using hot pressing the electrodes onto the membrane at 135 °C under a pressure of 60 atm for 2 minutes. MEA was made from commercial Pt/C catalyst at the same conditions above.

The prepared MEAs were installed in the fuel cell test station (FCT-1505 by BIO-LOGIC SA) and tested at a backpressure 1 atm on both sides and flow rates 500 mL/min and 300 mL/min for oxygen and hydrogen, respectively. Other operational parameters will be mentioned in each test as they change accordingly.

### 3. Model Validation Using Non-precious Catalyst Data

At this stage, the current model was validated against NG-based cobalt data calculated at the previous stage (Table 1). To match the model results with the produced experimental data, an adjusting parameter was used as coefficient in the Butler-Volmer equation (Table 1). The current model was validated against experimental data for NG-based cobalt in Fig. 2. As can be seen over the entire range of the polarization curve, a very good agreement was achieved between the model results and experiment data. There were error

**Table 1. The values of input parameters for non-precious catalyst (base case conditions)**

| Parameters | Quantity | Value/Units |
|---|---|---|
| T | Temperature | 80 °C |
| P | Pressure | 1.0 atm |
| $X_{O_2}$ | Oxygen mole fraction in CCL | 100% |
| s | Liquid water saturation | 0.5 |
| $t_{CL}$ | Catalyst layer thickness | 30 μm |
| $m_{Co}$ | Co mass loading | 0.01 kg $m^{-2}$ |
| $\rho_{Co}$ | Cobalt density | 8746 kg $m^{-3}$ |
| $\rho_{NG}$ | NG density | 2000 kg $m^{-3}$ |
| $\rho_i$ | Ionomer density | 1800 kg $m^{-3}$ |
| $r_{Co/NG}$ | Cobalt mass ratio on Co/NG particles | 0.4 |
| $\alpha_C$ | Transfer factor of cathode | 0.4 |
| $\alpha_a$ | Transfer factor of anode | 0.4 |
| $\kappa$ | Protonic conductivity [17] | 17 $\Omega^{-1}m^{-1}$ |
| $\sigma$ | Electronic conductivity [17] | 72,700 $\Omega^{-1}$ $m^{-1}$ |
| $\tau$ | CL tortuosity [18] | 1.5 |
| $r_{agg}$ | Radius of agglomerate | 0.7 μm |
| $\varepsilon_{agg}$ | Spherical agglomerate porosity | 0.45 |
| $\delta_{agg}$ | Thickness of agglomerate | 30 nm |
| $\varepsilon_{CL}$ | CL porosity | 0.2 |
| $\varepsilon_g$ | GDL porosity [19] | 0.74 |
| $L_{GDL}$ | GDL Thickness | 310 |
| $L_{mc}$ | Volume fraction of membrane in the CL | 0.3 |
| $L_{gc}$ | Volume fraction of GDL in the CL [20] | 0.05 |
| ECSA | Electrochemical surface area | $43*10^3$ |
| $i_0$ | Exchange current density | $1.26*10^{-7}$ A/$m^2$ if V>0.8<br>$1.1*10^{-5}$ if V<0.8 |
| AP | Adjusting parameter | Ap=100 if V>0.8<br>Ap=4.0 if V<0.8 |

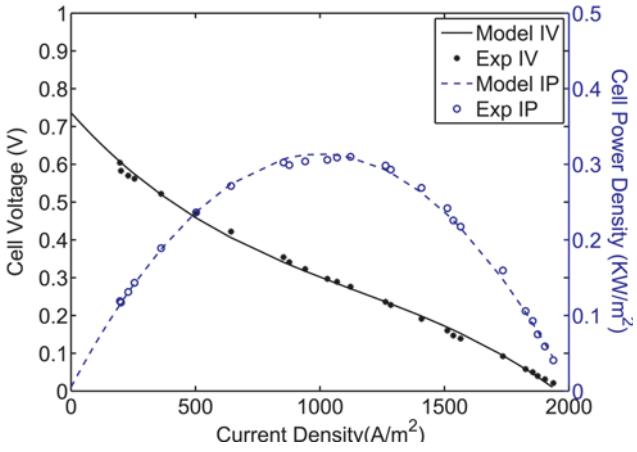


**Fig. 2. Comparing the current model and our experimental data of non-precious catalyst (80 °C, 1 atm, RH 100%).**

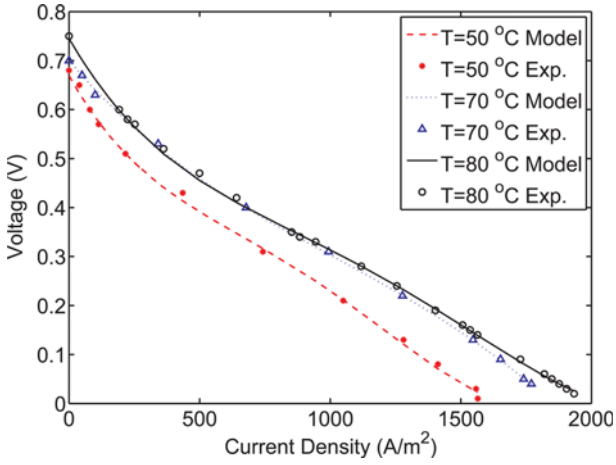


**Fig. 4. Comparison of the model I-V curves and Co/NG points at RH of 100%, 1 atm and three temperatures.**

values between the model results and the experiment data as 1.9%, 1.3% and 0.45% at the beginning, middle and end of the polarization curve, respectively.

**4. Operational Parameters Survey of the Model**

In the previous section, the model was verified against a set of data at constant operational parameters. Next we investigated the model at different values of these variables to show more reliability. First, it's shown how the model predicts changes in relative humidity. The fuel cell station was run at various relative humidity to produce data in order to compare the simulated results. Polarization curves for experimental data and simulated ones are plotted in Fig. 3 at three levels of relative humidity 60%, 80%, and 100%. The fuel cell temperature and pressure were set at 80 °C and 1 atm, respectively. As can be seen in Fig. 3, the model correctly predicts the fuel cell behavior when relative humidity changes. Also, in all curves an increase in relative humidity, which helps to keep the membrane wet enough especially at the anode side to facilitate proton transport, leads to an increase in the current density.

Second, the model was run to test its stability against changes in the temperature. The effect of temperature on fuel cell performance is drawn in Fig. 4 for both experimental and simulated results. Polarization curves are drawn in relative humidity of 100% and pressure of 1 atm and three different temperatures. As demonstrated in Fig. 4, there is a good agreement between experimental data and simulated ones. Moreover, in constant relative humidity, when the temperature increases, the thermal energy available in the system also increases such that particles become more active and with increased intensity, so there is greater probability of reactants reaching an activated state [21]. Thus, the reaction rate climbs up; as a result, the current density increases. Furthermore, increasing the temperature leads to reduction of the liquid phase and therefore the oxygen diffusion coefficient is further increased. As seen in Fig. 4, at moderate voltages, increasing the temperature by more than 70 °C does not enhance the performance, so 70 °C is the optimum temperature at these conditions. Having relied on the results of this modeling, the following optimization results can be conducted.

**5. Comparison of the NG-based Cobalt Catalyst with Platinum**

The NG-based cobalt catalyst is compared with platinum through application in a cell under the same conditions as the polarization curves shown in Fig. 5. As seen, the current density of NG-based

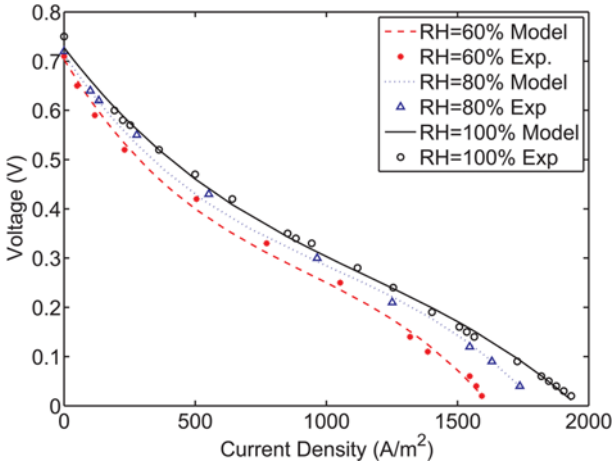


**Fig. 3. Comparison of the model I-V curves and Co/NG points at 80 °C, 1 atm and three levels of relative humidity.**

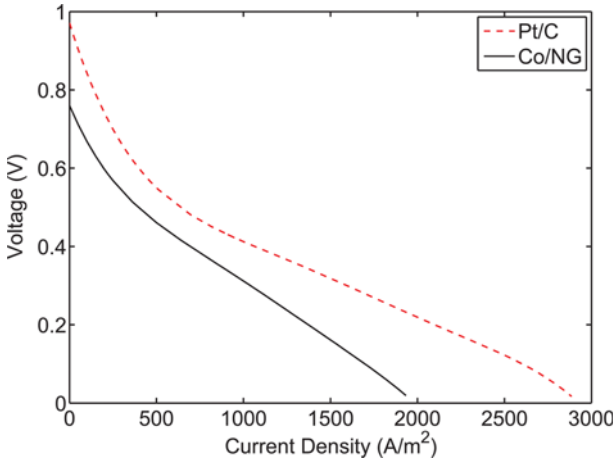


**Fig. 5. The polarization curves of NG based cobalt catalyst and Pt/C: 1 mg/cm$^2$, RH of 100%, 1 atm and 80 °C.**

cobalt reached 66% that of platinum at the voltage of 0.4 V, and its limited current density reached 67% that of platinum. Open circuit voltage (OCV) of NG-based cobalt was 0.75 V in 80 °C, while OCV of platinum was 0.94 V.

The catalyst layer plays a crucial role in defining the performance of the fuel cell. Moreover, the size and application of the fuel cell largely contributes to what extents the catalyst layer defines the MEA performance. Generally, the catalyst layer accounts for 77% of the total cost of a PEM fuel cell stack according to the annual report of DOE in 2005 [22]. The involved technologies, though, are growing rapidly resulting in the reduction of the relevant costs. According to Alaswad [23], the catalyst layer constituted about 68%, 46%, and 35% of the cost of a fuel cell stack with high volume production in 2006, 2010, and 2015, respectively. In this paper, the cost of Pt/C and NG based cobalt catalysts contributes 56% and 51% to the stack cost. Since the contribution of the non-precious catalyst is still high, it is simply not priced competitively unless its performance climbs. It is important to mention that we used the 1 mg/cm$^2$ loading for both catalysts in order to have identical conditions. But, due to the lower price of cobalt catalyst it could be employed more catalyst loading in the future work.

**6. The Polarization Curves in Base Case and Optimized Case**

The polarization curves are plotted in base case and optimized case in Fig. 6. One of the objective functions, namely cost, is considered equal to the base cost and another, namely performance is optimized. Although the amount of increase in the catalyst layer performance is more at high current density, its relative increase is less.

**7. Pareto Curve (Performance-cost Tradeoff)**

In Fig. 7, a Pareto curve is shown to optimize objectives of performance and the cost of catalyst layer at the voltage of 0.6 V (each voltage can be considered), in which the base case is marked as a circle. When multi objective optimization was applied to the base case at the same voltage and the current density, at first the cost suddenly fell compared to the base case and then it gradually grew according to increased current density. As observed, the slope of the curve is very smooth on the left side of the graph; this means that any increase in current density will not lead to a steep rise in cost; therefore the current density can be increased as necessary.

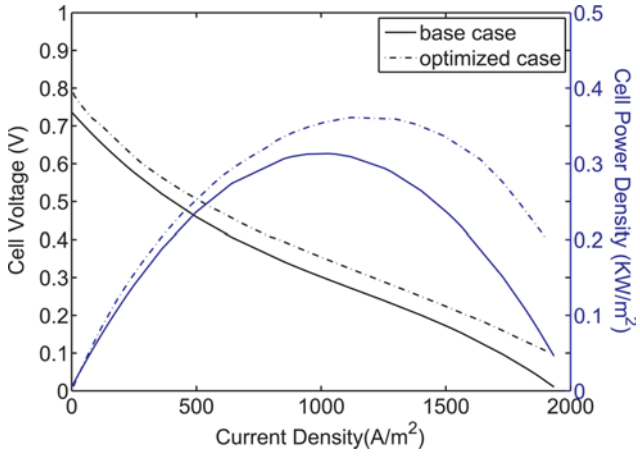


**Fig. 6. The polarization and power curves of the fuel cell in the base case and optimized case.**

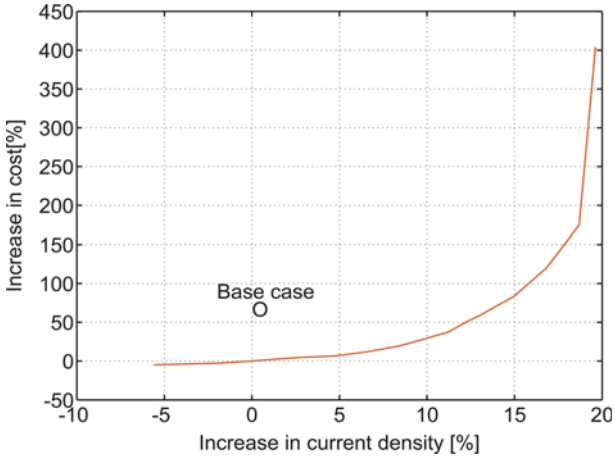


**Fig. 7. Pareto curve for MOO of Co/NG based catalyst layer at the voltage of 0.6 V.**

However, on the right side of the graph a small increase in current density leads to a high rise in cost, meaning an increase in performance will not be affordable in this region. Consequently, any tradeoff between cost and performance should be done in the middle of the curve where the current density increases in the range of 5% to 15%. In this region the optimization objectives meet simultaneously, i.e., the optimized current density is more than the base case and the optimized cost is less than the base case.

## CONCLUSION

Non-precious catalyst of NG-based cobalt was synthesized according to our previous work [4]. Next, the catalyst layer was made by using an airbrush and then membrane electrode assembly (MEA) was fabricated by a hot press machine. Operational tests for produced MEA were done in a cell, and in addition to MEA evaluation, the required empirical data were produced for validation of the catalyst layer optimization. In the modeling stage, the derived nonlinear equations were solved by the shooting method through coding in MATLAB software. Finally, at the optimization stage, the objective functions of the current density and cost were optimized using a multi-objective optimization through a sequential quadratic programming and min-max method. The decision variables included cobalt loading, ionomer volume fraction, agglomerate porosity and radius, and water saturation. Synthesized non-precious catalyst was evaluated in a cell and compared to platinum. The results showed that expensive platinic catalysts could be replaced by non-precious catalysts. Moreover, the performed modeling was in a good agreement with NG cobalt catalyst data. Afterwards, a polarization curve was plotted in both the base case and the optimized case. Lastly, the Pareto curve at the voltage of 0.6 V indicated the best tradeoff between cost and performance of the catalyst layer was achieved when the current density increased in the range of 5% to 15%.

## NOMENCLATURE

AP : adjusting parameter

c : concentration [mol $m^{-3}$]
CL : catalyst layer
$C_1$, $C_2$ : coefficients for costs
$f_1$, $f_2$ : objective functions
I : local current density [A $m^{-2}$]
$I_0$ : exchange current density [A $m^{-2}$]
$I_\delta$ : cell current density [A $m^{-2}$]
IV : current density versus voltage
IP : current density versus power density
$t_{LC}$ : catalyst layer thickness [m]
Lgc : volume fraction of GDL penetrating into the CL
$L_{mc}$ : volume fraction of ionomer phase in the CL
$m_{Co}$ : cobalt mass loading [kg $m^{-2}$]
P : pressure [atm]
Pt/C : platinum/carbon catalyst
$r_{agg}$ : agglomerate radius [m]
$r_{Co/NG}$ : mass fraction of cobalt to Co/NG particles
RH : relative humidity
s : liquid water saturation
T : temperature [K]
t : thickness
W : weight

**Greek Letters**

$\delta_{agg}$ : ionomer film thickness [m]
$\varepsilon_{agg}$ : spherical agglomerate porosity
$\varepsilon_{CL}$ : CL porosity
$\varepsilon_g$ : GDL porosity
$\varepsilon_i$ : volume fraction of ionomer
$\varepsilon_s$ : volume fraction of solids
$\varepsilon_v$ : volume fraction of voides
$\rho_{NG}$ : NG density [kg $m^{-3}$]
$\rho_{Co}$ : Cobalt density [kg $m^{-3}$]
$\rho_i$ : ionomer density [kg $m^{-3}$]
$\sigma$ : electronic conductivity [S $m^{-1}$]
$\kappa$ : protonic conductivity [S $m^{-1}$]
$\tau$ : CL tortuosity

**Subscriptions**

a : anode
c : cathode
agg : agglomerate
CL : catalyst layer
Co : cobalt
NG : nitrogen doped graphene
I : ionomer

## REFERENCES


1. C. Spiegel, *PEM fuel cell modeling and simulation using Matlab*, Elsevier Inc. (2008).
2. D. P. Wilkinson, J. Zhang, R. Hui, J. Fergus and X. Li, *Proton Exchange Membrane Fuel Cells: Materials Properties and Performance*, Taylor and Francis Group LLC (2010).
3. R. Othman, A. L. Dicks and Z. Zhu, *Int. J. Hydrogen Energy*, **37**, 357 (2012).
4. H. Ghanbarlou, S. Rowshanzamir, B. Kazeminasab and M. J. Parnian, *J. Power Sources*, **273**, 981 (2015).
5. K. Broka and P. Ekdunge, *J. Appl. Electrochem.*, **27**, 281 (1997).
6. P. C. Sui, L. D. Chen, J. P. Seaba and Y. Wariishi, *SAE Congress*, **01**, 61 (1999).
7. Q. Wang, D. Song, T. Navessin, S. Holdcroft and Z. Liu, *Electrochim. Acta*, **50**, 725 (2004).
8. W. Sun, B. A. Peppley and K. Karan, *Electrochim. Acta*, **50**, 3359 (2005).
9. M. Srinivasarao, D. Bhattacharyya, R. Rengaswamy and S. Narasimhan, *Chem. Eng. Res. Des.*, **89**, 10 (2011).
10. A. A. Kulikovsky, *Electrochim. Acta*, **79**, 31 (2012).
11. S. O. Mert and Z. Özçelik, *Int. J. Energy Res.*, **37**, 1256 (2013).
12. M. S. Feali and M. Fathipour, *Russian J. Electrochem.*, **50**, 561 (2014).
13. S. M. C. Ang, D. J. L. Brett and S. Fraga, *J. Power Sources*, **195**, 2754 (2010).
14. J. C. Park, S. H. Park, M. W. Chung, C. H. Choi, B. K. Kho and S. I. Woo, *J. Power Sources*, **286**, 166 (2015).
15. D. Malko, T. Lopes, E. A. Ticianelli and A. Kucernak, *J. Power Sources*, **323**, 189 (2016).
16. B. Kazeminasab, S. Rowshanzamir and H. Ghadamian, *Bulgarian Chem. Commun.*, **47**, 38 (2015).
17. M. Moein-Jahromi and M. J. Kermani, *Int. J. Hydrogen Energy*, **37**, 17954 (2012).
18. S. Inamuddi, T. A. Cheema, S. M. J. Zaidi and S. U. Rahman, *Renewable Energy*, **36**, 529 (2011).
19. S. Obut and E. Alper, *J. Power Sources*, **196**, 1920 (2011).
20. N. Khajeh-Hosseini-Dalasm, M. Fesanghary, K. Fushinobu and K. Okazaki, *Electrochim. Acta*, **60**, 55 (2012).
21. R. O'Hayre, S. W. Cha, W. Colella and F. B. Prinz, *Fuel Cell Fundamentals*, New York, Wiley (2006).
22. J. Zhang, *PEM fuel cell electrocatalysts and catalyst layers*, Springer (2008).
23. A. Alaswad, A. G. Olabi, A. Palumbo and M. Dassisti, *PEM Fuel Cell Cost Analysis during the Period (1998-2014)*, Elsevier (2016).